Supporting Information

Enhancing Intermolecular Packing and Light Harvesting through Asymmetric Non-Fullerene Acceptors for Achieving 18.7% Efficiency Ternary Organic Solar Cells

Zhiliang Zhang,[a,‡] Jingnan Wu,[a,d,‡] Ji Lin,[a] Rui Zhang,[c] Junfang Lv,[a] Linfeng Yu,[a] Xia Guo,[b*] Maojie Zhang[a,b*]

[a]Laboratory of Advanced Optoelectronic Materials, Suzhou Key Laboratory of Novel Semiconductor-optoelectronics Materials and Devices, College of Chemistry, Chemical Engineering and Materials Science, Soochow University, Suzhou 215123, China

E-mail: mjzhang@sdu.edu.cn (M. J. Zhang)

[b]National Engineering Research Center for Colloidal Materials, School of Chemistry & Chemical Engineering, Shandong University, Jinan, Shandong 250100, China

E-mail: guoxia0610@sdu.edu.cn (X. Guo)

[c]Department of Physics, Chemistry and Biology (IFM), Linköping University, Linköping, Sweden

[d]Department of Chemistry and Bioscience, Aalborg University, DK-9220 Aalborg, Denmark

‡The authors contributed equally to this work

Corresponding Author

* E-mail: mjzhang@sdu.edu.cn (M. J. Zhang); guoxia0610@sdu.edu.cn (X. Guo)

Experimental

Materials

All chemicals and solvents were reagent grades and purchased from Damas-beta, Acros Organics, and Sigma-Aldrich. PM6 was synthesized according to the previous literature.[1] BTP-eC9 was purchased from Solarmer Materials Inc. Compound 1 and compound 2 were purchased from Derthon Optoelectronic Materials Science Techology Co.,Ltd.

AFIC was synthesized as follows:
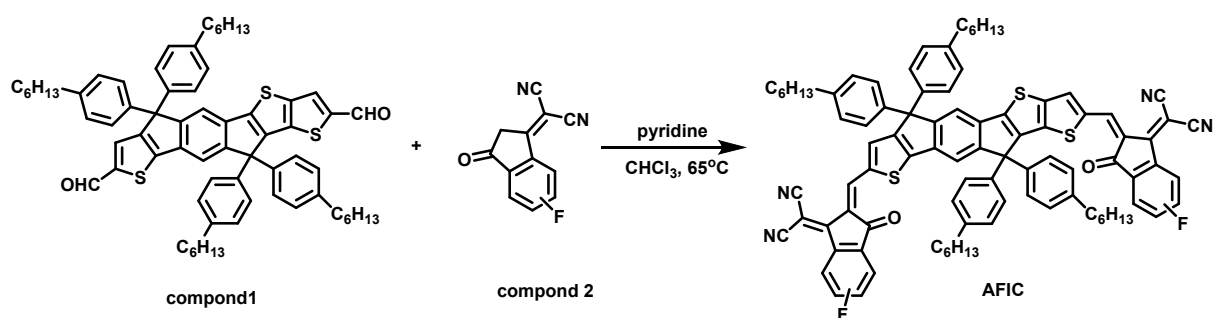
Scheme S1 Synthetic route of the AFIC.

Compound 1 (0.30 g, 0.29 mmol), Compound 2 (0.19 g, 0.89 mmol), pyridine (0.5 mL) and chloroform (30 mL) were dissolved in a round bottom flask under nitrogen. The mixture was stirred at 65 °C for 12 h. After cooling to room temperature, the mixture was poured into methanol and filtered. The residue was purified with column chromatography on silica gel using dichloromethane/petroleum ether (1/1, v/v) as the eluent to give a dark aubergine solid AFIC (0.27g, 66%). ^{1}H NMR (400 MHz, CDCl$_3$) δ 8.89-8.88 (d, 1 H), 8.86 (s, 1 H) 8.72-8.69 (m, 1 H), 8.38-8.36 (d, 1 H), 8.23-8.21 (d, 1 H), 7.94-7.89 (m, 1 H), 7.78 (s, 1 H), 7.71-7.72 (d, 1 H), 7.59 (s, 1 H), 7.56-7.53 (m, 1 H), 7.43-7.39 (t, 2 H), 7.21-7.19 (d, 4 H), 7.17-7.11(m, 12 H), 2.59-2.56 (t, 8 H), 1.64-1.57 (m, 10 H), 1.36-1.26 (m, 24 H), 0.89-0.84 (m, 10 H). ^{13}C NMR (101 MHz, CDCl$_3$) δ 185.65, 167.02, 164.45, 164.01, 156.92, 155.51, 154.77, 147.16, 146.27, 143.01, 141.59, 141.39, 140.11, 140.07, 139.26, 138.75, 137.77, 137.59, 137.31, 136.08, 132.08, 127.91, 127.75, 126.89, 126.79, 126.70, 125.01, 121.71, 118.78, 117.86, 113.18, 111.65, 76.32, 76.00, 75.68, 69.35, 68.93, 62.23, 61.98, 34.57, 34.53, 30.68, 30.29, 30.22,

28.12, 28.07, 21.56, 13.07. MS (MALDI) $C_{88}H_{78}N_4O_2S_5$: m/z calc.1407.54, found 1406.36.

Device fabrication and characterization

Device fabrication:

Organic solar cells were fabricated on ITO glass substrates with the conventional structure of ITO/PEDOT:PSS (30 nm)/Active layer/PFN-Br (5 nm)/Al (100 nm). The patterned indium tin oxide (ITO) coated glasses was cleaned by detergent and then underwent a wet-cleaning process inside an ultrasonic bath procedure, following by ultrapure water, acetone and isopropanol in sequence and then dried in an oven overnight to remove the residual solvents. The precleaned ITO substrates were treated in UV-ozone for 20 min, and then diluted PDEOT:PSS (Heraeus Clevios P VP. AI 4083) were spin-coated on top of ITO at 6000rpm for 40s, and thermal annealed at 150 °C for 15 min under air atmosphere. Afterward, the ITO substrates coated with PEDOT:PSS film were transferred into a nitrogen-purged glove box. The optimal PM6:BTP-eC9 (1:1.2, weight ratio), PM6:AFIC (1:1.2, weight ratio) and PM6:BTP-eC9:AFIC (1:1.2:0.1, weight ratio) were all dissolved in chloroform with a polymer weight concentration of 8 mg/mL, dissolved for at least 4 h on the hotplate with 40 °C. Before the spin coating process, 0.5% 1,8-diiodooctane (v/v) was added to the solutions. The blend solution was spin-cast at 3000-4000 rpm for 40 s over the ITO glasses to form an active layer. Subsequently, the blend films were heated at 100 °C for 10 min. Then, solution of PFN-Br which dissolved in methanol with a concentration of 0.5 mg/mL was spin-coated over the active layers at 3000 rpm for 35 s. Finally 100 nm Al layer were deposited on the active layers under vacuum at a pressure of ca. 4×10^{-4} Pa through a shadow mask to determine the active area of the devices (~0.04 cm^2).

Device characterization:

Device current density-voltage (*J-V*) characteristics were recorded using a Keithley 2450 Source Measure Unit. The PCE values of the PSCs were measured under illumination of AM 1.5G (100 mW cm^{-2}) using a SS-F5-3A solar simulator (AAA grade, 50 × 50 mm^2 photobeam

size) of Enli Technology CO., Ltd. A 2×2 cm^2 monocrystalline silicon reference cell (SRC-00019) was purchased from Enli Technology CO., Ltd. The EQE was measured by Solar Cell spectral Response Measurement System QE-R3011 of Enli Technology CO., Ltd. The light intensity at each wavelength was calibrated with a standard single-crystal Si photovoltaic cell.

Instruments and measurements

^{1}H NMR and ^{13}C NMR spectra were collected on a Bruker AV 400 MHz FT-NMR spectrometer with tetramethylsilane (TMS) as the internal standard and CDCl3 as the solvent. Elemental analysis of the polymers was conducted on the Flash EA1112 analyzer.

UV-Vis absorption and cyclic voltammetry

Absorption spectra of materials were performed on a UV-Vis-NIR Spectrophotometer (Agilent Technologies Carry 5000 Series). Cyclic voltammetry (CV) was performed on a Zahner Zennium IM6 electrochemical workstation with a three-electrode system in 0.1 mol L^{-1} Bu$_4$NPF$_6$ acetonitrile solutions at a scan rate of 50 mV s^{-1}.

Contact angle measurement

Contact angles of distinct solvents (deionized water and diiodomethane) on polymer donor PM6, non-fullerene acceptors BTP-eC9 and AFIC films were measured by using Dataphysics-OCA20 Micro surface contact angle analyzer. The surface tension of the polymers was characterized and calculated by the contact angles of the two probe liquids (ultrapure water and diiodomethane) with the Owens and Wendt equation: $\gamma_{LV}(1 + \cos\theta) = 2(\gamma_S{}^d\gamma_L{}^d)^{1/2} + 2(\gamma_S{}^p\gamma_L{}^p)^{1/2}$, where γ_S and γ_L are the surface energy of the sample and the probe liquid, respectively. The superscripts d and p refer to the dispersion and polar components of the surface energy, respectively.

DSC and PL measurement

Differential scanning calorimetry (DSC) was performed on a TA DSC Q-200. Ultraviolet-visible-near infrared (UV-Vis-NIR) absorption spectra was taken on an Agilent Technologies

Cary 5000 Series UV-Vis-NIR Spectrophotometer. Photoluminescence (PL) spectra was performed on an Edinburgh Instrument FLS 980.

SCLC Mobility Measurement

The hole and electron mobilities of devices were evaluated from space-charge-limited current (SCLC) method with hole-only structure of ITO/PEDOT:PSS/Active layer/MoO_3/Al and electron-only structure of ITO/ZnO/ Active layer/PFN-Br/Al, respectively. The corresponding charge mobilities were calculated from fitting the Mott-Gurney square law $J = 9\varepsilon_r\varepsilon_0\mu V^2/(8L^3)$, where J is the current density, ε_r is the dielectric permittivity of the active layer (assumed to be 3), ε_0 is the vacuum permittivity, L is the thickness of the active layer, μ is the hole or electron mobility. $V = V_{appl} - V_{bi} - V_s$, V_{appl} is the applied voltage, V_{bi} is the built-in voltage, V_s is the voltage drop from the substrate's series resistance ($V_s = IR$). The SCLC devices were measured under a dark condition in a nitrogen glovebox without encapsulation.

AFM and TEM characterization

Atomic force microscopy (AFM) was performed by Dimension 3100 (Veeco) Atomic Force Microscope at tapping mode. Transmission electron microscopy (TEM) was measured by Tecnai G2 F20 S-TWIN instrument (accelerating voltage, 200 kV), in which the blend films were prepared as following: the blend films were spin coated on the PEDOT:PSS-based substrates and then were immersed in deionized water to obtain floated BHJ films, and finally unsupported 200 mesh copper grids was used to pick films up.

TPC and TPV measurement

Transient photovoltage (TPV) and transient photocurrent (TPC) measurements were carried out under a 337 nm 3.5 ns pulse laser (160 μJ per pulse at 10 Hz) and halide lamps (150 W). Voltage and current dynamics were recorded on a digital oscilloscope (Tektronix MDO3102).

GIWAXS measurements

Grazing incident wide-angle X-ray scattering (GIWAXS) data was obtained from NCD-

SWEET beamline, ALBA Synchrotron, Spain. The energy of the X-ray beam was set to 12.95 keV using a Si (111) channel-cut monochromator and further collimated with an array of Be lenses. The incidence angle was 0.14° and the diffraction patterns were collected using a Rayonix LX255-HS area detector, which consists of a pixel array of 5760×1920 (V×H) with a pixel size of 88.54×88.54 μm^2 for the pixel binning employed of 2×2. The scattering vector q was calibrated using Cr_2O_3 as standard, obtained using a sample to detector distance of 0.23 m.

Supplementary figures and tables
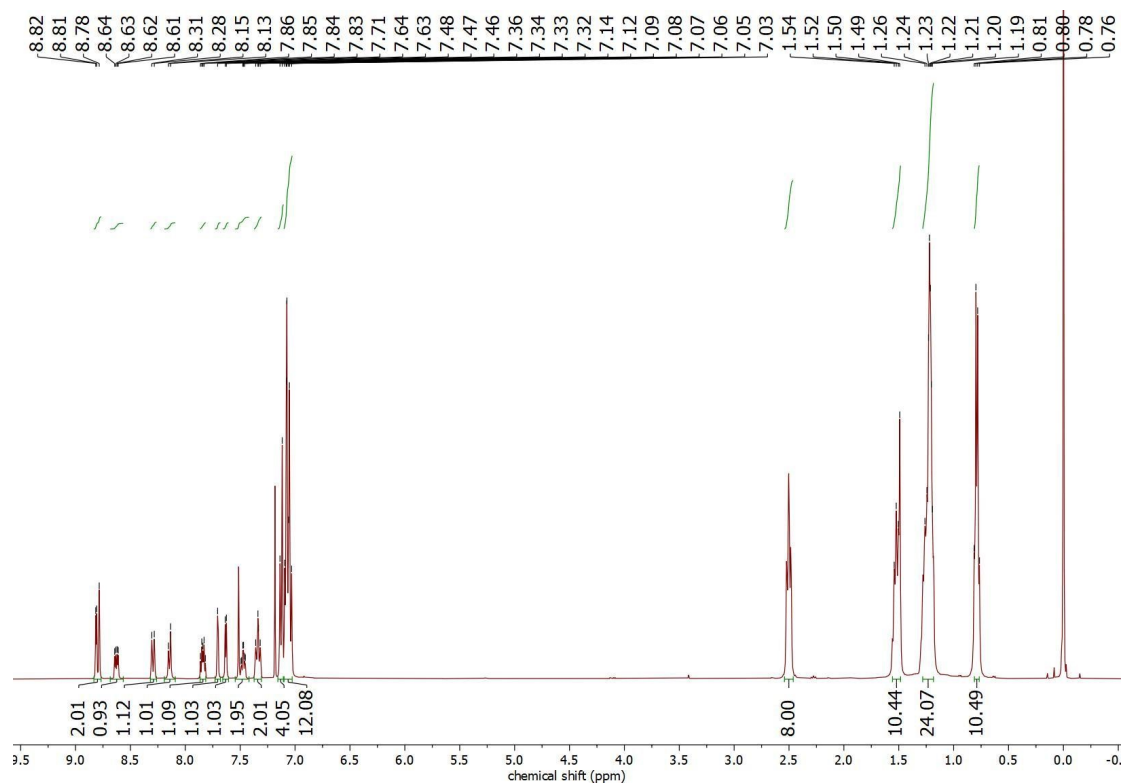
Fig. S1 ¹H NMR spectra of AFIC.
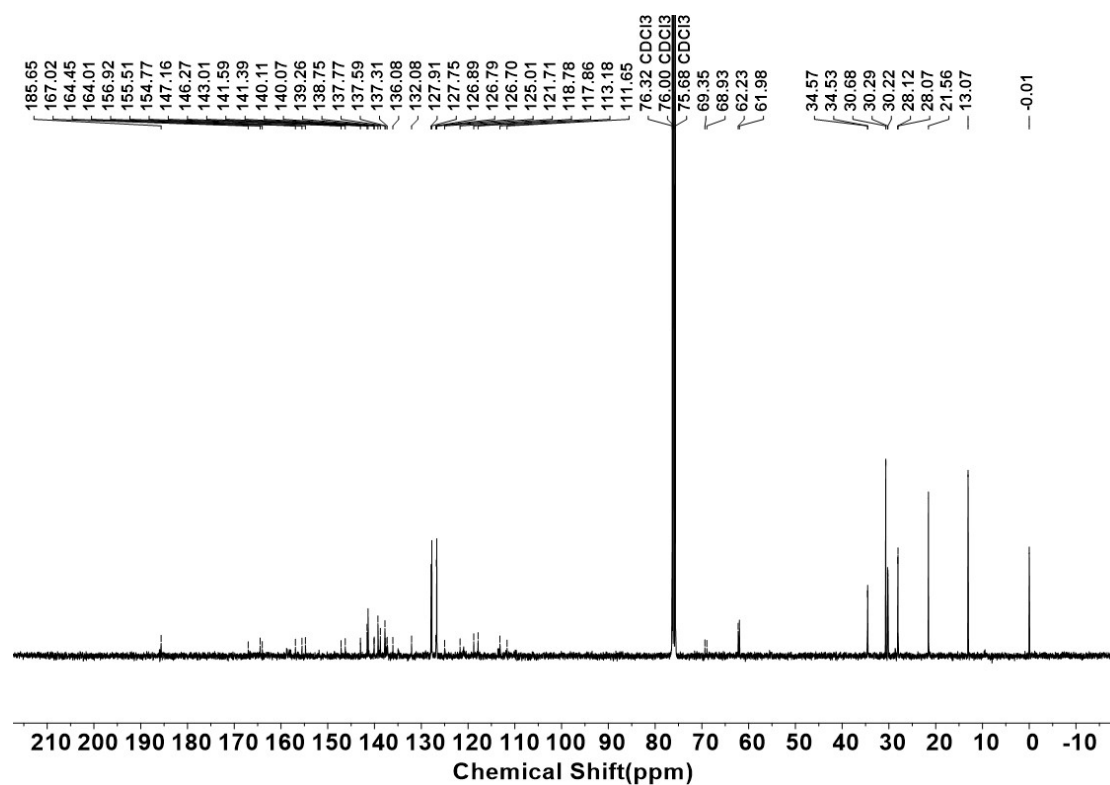
Fig. S2 ¹³C NMR spectra of AFIC.
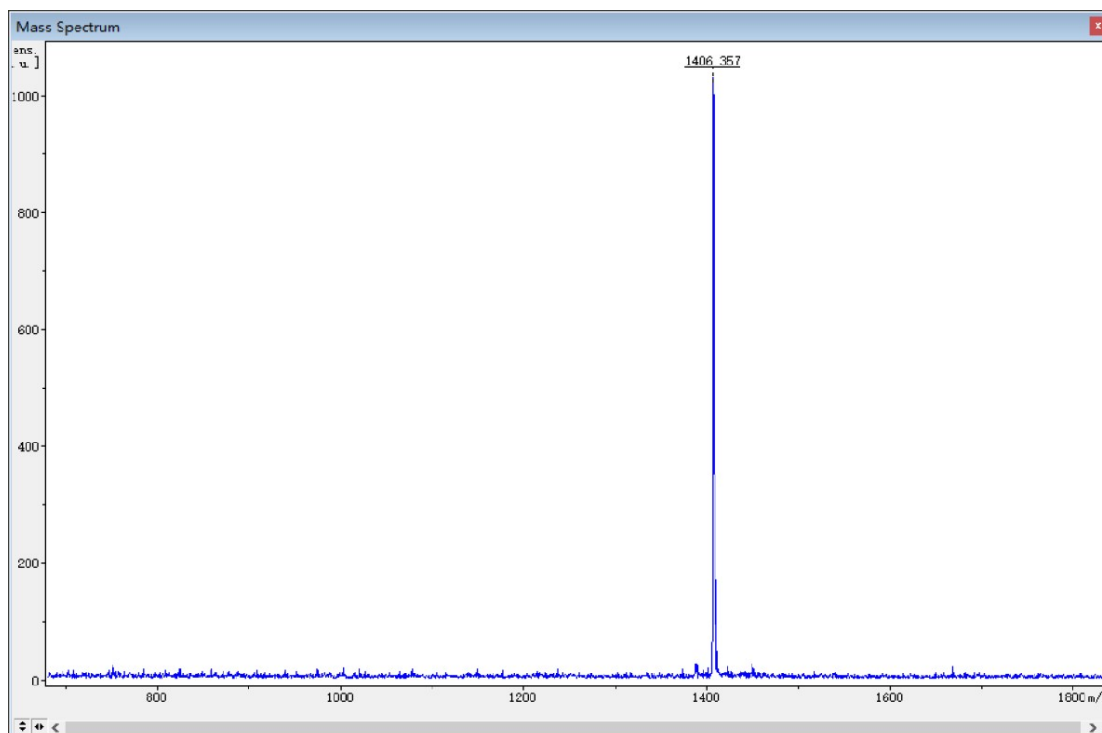
Fig. S3 MS-MALDI spectra of AFIC.
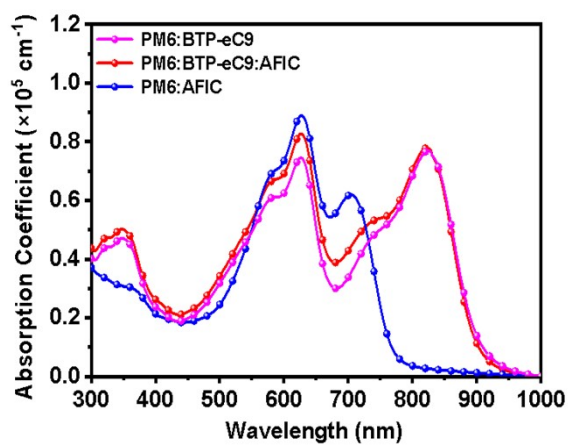
Fig. S4 Absorption coefficient of binary and ternary blend films.
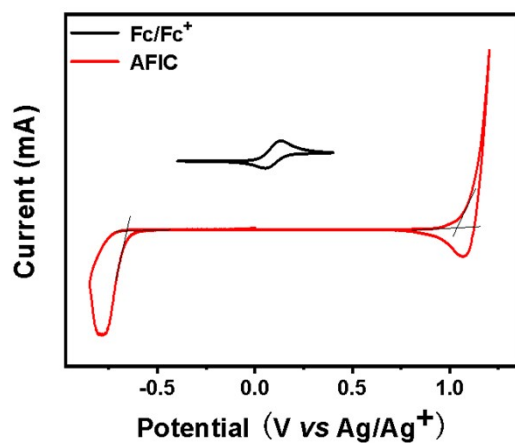
Fig. S5 Cyclic voltammograms of AFIC and Fc/Fc⁺.
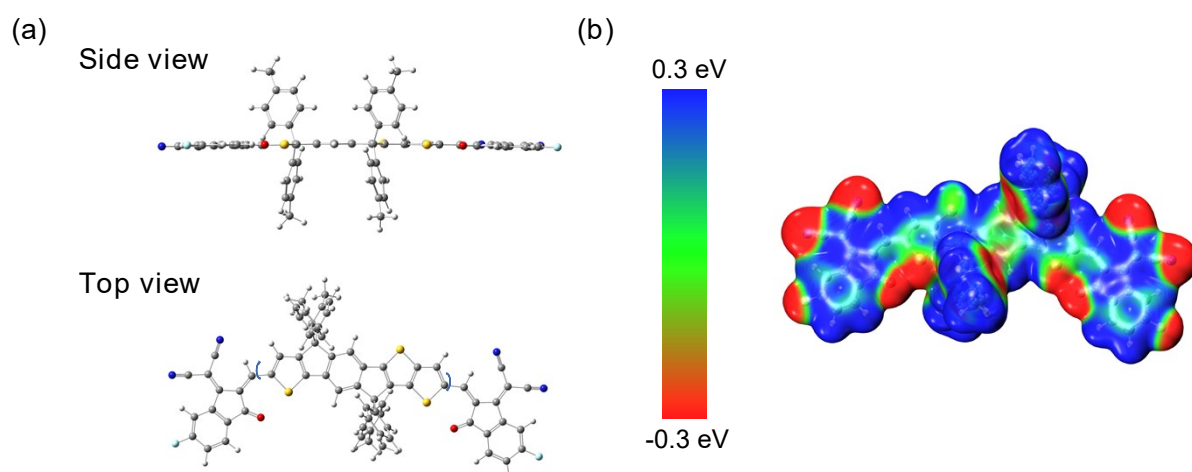
Fig. S6 (a) Molecular geometries of AFIC. (b) Electrostatic potential (ESP) maps of AFIC molecular.
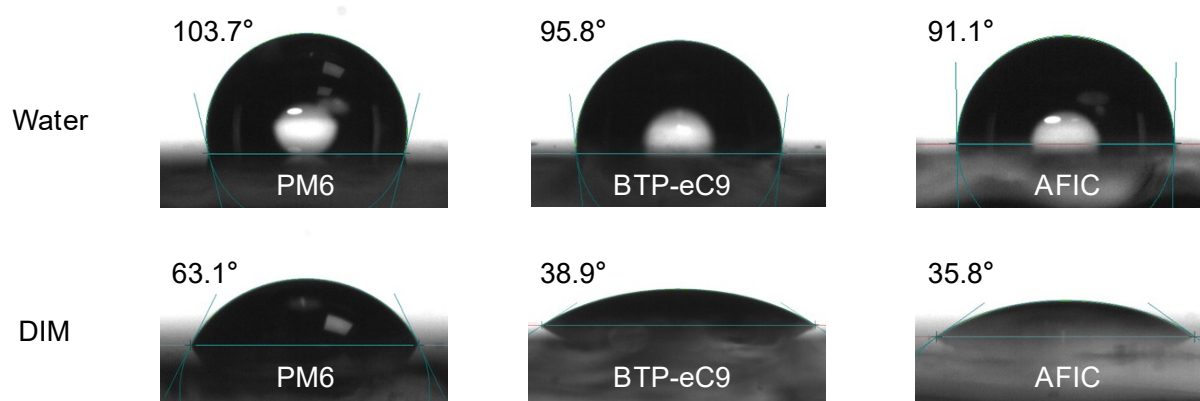
Fig. S7 Contact angle images of water and diiodomethane (DIM) droplets on PM6, BTP-eC9, AFIC neat films.
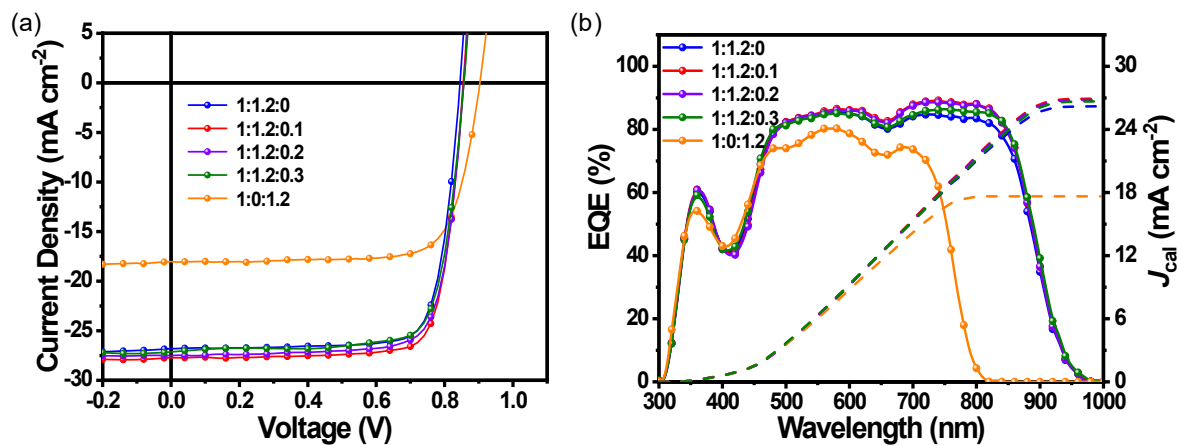
Fig. S8 (a) *J-V* curves and (b) EQE spectra of OSCs based on PM6: BTP-eC9:AFIC BHJ with various ratio of donor and acceptor.
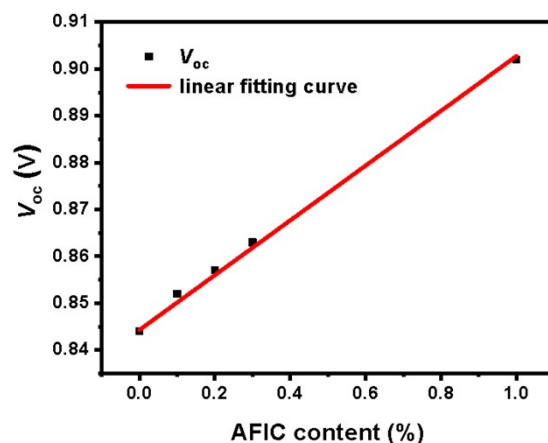
Fig. S9 V_{oc} variation curves of the ternary devices with different AFIC contents.
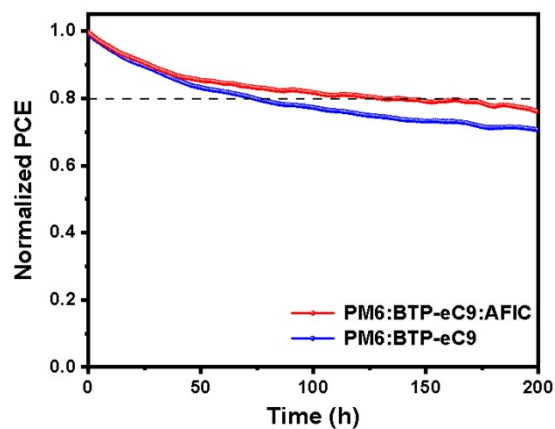
Fig. S10 Light stability behaviors of the corresponding OSCs with MPP tracking under continuous illumination in a nitrogen-filled glovebox.
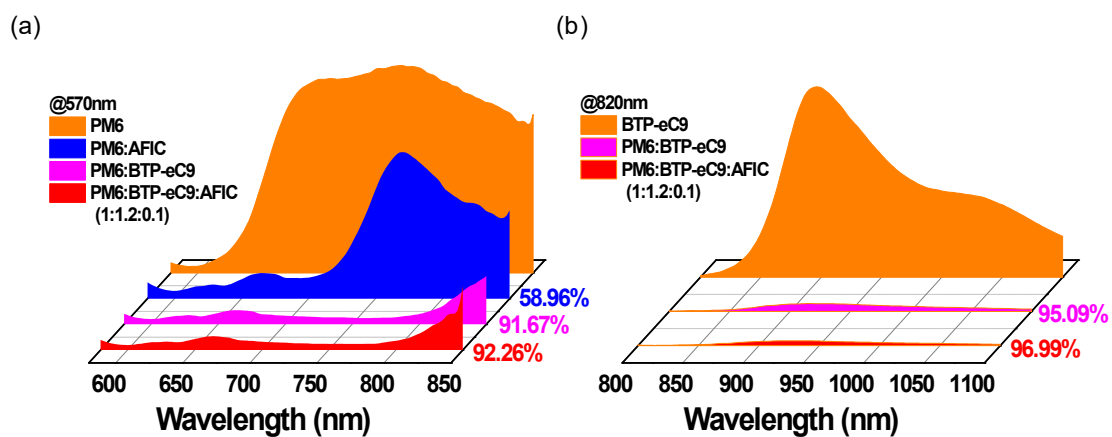
Fig. S11 PL intensities of neat donor PM6, acceptor BTP-eC9 films, and related blend films, excited at (a) 570 nm and (b) 820 nm.
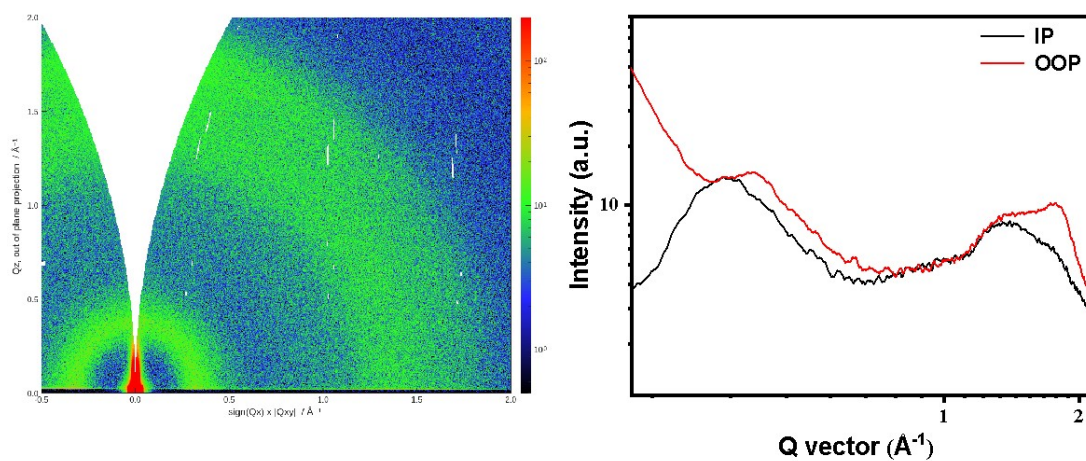
Fig. S12 2D GIWAXS patterns and corresponding line-cuts of the neat AFIC film.

Table S1. Summary of photovoltaic parameters of recent OSCs based on the asymmetric non-fullerene acceptors.

Acceptor	Active layer	V_{oc} (V)	J_{sc} (mA cm^{-2})	FF (%)	PCE (%)	Ref.
Y6-1O	PM6:Y6-1O	0.898	17.85	65.40	10.48	2
	PM6:Y7-BO:Y6-1O	0.867	26.35	79.27	18.11	
TB-S1-O	PM6:TB-S1-O	1.120	13.62	60.0	9.09	3
	PM6:BTP-eC9:TB-S1-O	0.857	27.40	77.2	18.14	
WA1	PM6:WA1	0.860	22.65	79.31	15.45	4
	PM6:Y6:WA1	0.870	27.68	75.36	18.15	
SN-O	D18:SN-O	0.925	20.1	63.9	11.9	5
	D18:Y6:SN-O	0.876	26.8	78.1	18.3	
AITC	PM6:AITC	1.07	14.3	71.6	11.0	6
	PM6:BTP-eC9:AITC	0.87	27.2	79.7	18.8	
BTP-2F2Cl	PM1:BTP-2F2Cl	0.861	27.35	78.16	18.40	7
	PM1:L8-BO:BTP-2F2Cl	0.881	27.15	80.14	19.17	
BTP-S10	PM6:BTP-S10	0.943	20.54	69.46	13.44	8
	PM6:BTP-eC9:BTP-S10	0.898	26.80	80.22	19.26	
BTP-S17	PM6:BTP-S17	0.978	20.78	68.17	13.89	9
	PM6:BTP-eC9:BTP-S17	0.873	27.59	79.55	19.19	
	PM6:BTP-eC9:BTP-S16:BTP-S17	0.881	27.75	80.83	19.76	
AFIC	PM6:AFIC	0.902	18.1	76.0	12.4	This work
	PM6:BTP-eC9::AFIC	0.854	27.7	79.0	18.7	

Table S2. Summary of contact angles (θ), surface tensions (γ), and Flory-Huggins interaction parameters (χ) for PM6, BTP-eC9, and AFIC films.

Sample	Contact angels		γ (mN m^{-1})	$\chi^{D,A}$ [a]	$\chi^{A_1-A_2}$ [b]
	θ_{water} (°)	θ_{DIM} (°)			
PM6	103.7	63.1	27.19	/	/
BTP-eC9	95.8	38.9	41.12	1.44κ	/
AFIC	91.1	35.8	41.96	1.60κ	0.004κ

[a] The Flory-Huggins interaction parameter between the donor (D) and acceptor (A) is calculated through the equation of: $\chi^{D-A} = \kappa(\sqrt{\gamma_D}-\sqrt{\gamma_A})^2$, where κ is a positive constant.

[b] The Flory-Huggins interaction parameter between the two acceptors (A$_1$ and A$_2$) is calculated through the equation of: $\chi^{A_1-A_2} = \kappa(\sqrt{\gamma_{A_1}}-\sqrt{\gamma_{A_2}})^2$, where κ is a positive constant.

Table S3. Photovoltaic parameters of PM6:BTP-eC9:AFIC based solar cells with different D/A ratios.

PM6:BTP-eC9:AFIC	V_{oc} (V)	J_{sc}/J_{cal}[a] (mA cm^{-2})	FF (%)	PCE (%)
1:1.2:0	0.845	26.8/26.2	77.6	17.5
1:1.2:0.1	0.854	27.7/26.9	79.0	18.7
1:1.2:0.2	0.857	27.6/26.8	76.3	18.1
1:1.2:0.3	0.861	27.2/26.7	76.1	17.8
1:0:1.2	0.902	18.1/17.6	76.0	12.4

[a] Integrated J_{cal} in parenthesis from the EQE curves.

Table S4. Summary of photovoltaic parameters of ternary OSCs based on the PM6:BTP-eC9 host system.

Third component	Type	V_{oc} (V)	J_{sc} (mA cm^{-2})	FF (%)	PCE (%)	Ref.
G6-BO		0.85	27.6	77.67	18.13	[10]
BTP-ICBCF3		0.853	27.4	77.8	18.2	[11]
L8-BO-F		0.853	27.35	80.0	18.66	[12]
ZY-4Cl	symmetric	0.863	27.40	79.0	18.69	[13]
isoIDTIC		0.866	27.30	80.4	19.0	[14]
LA23		0.858	28.03	79.50	19.13	[15]
TB-S1-O		0.857	27.40	77.2	18.14	[3]
BTP-S2		0.878	26.78	79.44	18.66	[16]
AITC		0.87	27.2	79.7	18.8	[6]
BTP-S17	asymmetric	0.873	27.59	79.55	19.19	[9]
BTP-S16		0.863	27.73	80.64	19.31	[9]
AFIC		0.854	27.7	79.0	18.7	This work

Table S5. Recent progress in the photostability in a nitrogen-filled condition of ternary OSCs.

Host blend	Third component	PCE (%)[a]	Storage stability		Ref.
			Time (h)	PCE/PCE$_0$ (%)[a]	
PBDB-TF:Y6:	PC$_{71}$BM[b]	17.6	100	70	[17]
PM6:Y6	ITIC-M[c]	18.13	168	70	[18]
PM6:Y6	TIT-2Cl[d]	18.18	12	76	[19]
PM6-Ir1:BTP-eC9	PC$_{71}$BM[e]	18.31	200	80.8	[20]
PM6:Y6	dT9TBO[f]	18.41	500	80	[21]
PM6:BTP-eC9	BTP-F[f]	18.45	142	80	[22]
PBDB-T-2F:BTP-eC9:	PC$_{71}$BM[g]	18.65	200	80	[23]
PM6:BTP-eC9	L8-BO-F[f]	18.66	50	80	[12]
PM6:BTP-eC9	ZY-4Cl[f]	18.69	63	80	[13]
PM6:BTP-eC9	isoIDTIC[h]	19.0	254	80	[14]
PM6:BTP-eC9	AFIC	18.7	130	80	This work

[a] The percentage of PCE after illumination vs. initial PCE. [b] The device architecture is ITO/ZnO/ active layer/a-MoO$_x$/Ag. [c] The device architecture is ITO/PEDOT:PSS/active layer/PFN-Br/Ag. [d] The device architecture is ITO/PEDOT:PSS/active layer (LBL) /PDIN/Ag. [e] The device architecture is ITO (chlorinated ITO anode)/active layer/PNDIT-F3N/Ag. [f] The device architecture is ITO/PEDOT:PSS/active layer/PNDIT-F3N/Ag. [g] The device architecture is ITO-Cl (ODCB and ODCB:H2O2)/active layer/PFN-Br/Al. [h] The device architecture is ITO/Cl-2PACz /active layer/PNDIT-F3N/Ag.

Table S6. The charge collection efficiencies and exciton dissociation probabilities of solar cells with different active layers.

Sample	P_{coll} (%)[a]	P_{diss} (%)[b]
PM6:BTP-eC9	89.8	97.9
PM6:BTP-eC9:AFIC (1:1.2:0.1)	91.3	99.1
PM6:AFIC	86.9	97.9

[a] The charge collection efficiencies. [b] The exciton dissociation probabilities.

Table S7. The hole mobilities (μ_h) and electron mobilities (μ_e) of the binary and ternary OSCs.

Sample	μ_h (cm² V⁻¹ s⁻¹)	μ_e (cm² V⁻¹ s⁻¹)	μ_h/μ_e
PM6:BTP-eC9	6.72×10^{-4}	7.18×10^{-4}	0.94
PM6:BTP-eC9:AFIC (1:1.2:0.1)	1.24×10^{-3}	1.26×10^{-3}	0.98
PM6:AFIC	3.94×10^{-4}	4.90×10^{-4}	0.80

Table S8. Detailed GIWAXS (010) peak information of three BHJ films.

Sample	q (Å⁻¹)	d-spacing (Å)	FWHM (Å⁻¹)	CCL (Å)
PM6:BTP-eC9	1.73	3.63	0.200	28.28
PM6:BTP-eC9:AFIC (1:1.2:0.1)	1.75	3.59	0.192	29.46
PM6:AFIC	1.77	3.55	0.205	27.64

Table S9. Detailed GIWAXS (100) peak information of three BHJ films.

Sample	q (Å⁻¹)	d-spacing (Å)	FWHM (Å⁻¹)	CCL (Å)
PM6:BTP-eC9	0.34	18.48	0.047	118.88
PM6:BTP-eC9:AFIC (1:1.2:0.1)	0.34	18.48	0.046	120.57
PM6:AFIC	0.34	18.48	0.038	148.58

References

1 M. Zhang, X. Guo, W. Ma, H. Ade and J. Hou, *Adv. Mater.*, 2015, **27**, 4655-4660.

2 H. R. Bai, Q. An, M. Jiang, H. S. Ryu, J. Yang, X. J. Zhou, H. F. Zhi, C. Yang, X. Li, H. Y. Woo and J. L. Wang, *Adv. Funct. Mater.*, 2022, **32**, 2200807.

3 L. Xie, A. Lan, Q. Gu, S. Yang, W. Song, J. Ge, R. Zhou, Z. Chen, J. Zhang, X. Zhang, D. Yang, B. Tang, T. Wu and Z. Ge, *ACS Energy Lett.*, 2022, **8**, 361-371.

4 P. Wang, Y. Li, C. Han, J. Wang, F. Bi, N. Zheng, J. Yang, J. Wang and X. Bao, *J. Mater. Chem. A*, 2022, **10**, 17808-17816.

5 R. Xu, Y. Jiang, F. Liu, W. Su, W. Liu, S. Xu, H. Fan, C. Jiang, Q. Zong, W. Zhang and X. Zhu, *Chem. Eng. J.*, 2023, **464**.

6 J. Wang, M. Zhang, J. Lin, Z. Zheng, L. Zhu, P. Bi, H. Liang, X. Guo, J. Wu, Y. Wang, L. Yu, J. Li, J. Lv, X. Liu, F. Liu, J. Hou and Y. Li, *Energy Environ. Sci.*, 2022, **15**, 1585-1593.

7 R. Sun, Y. Wu, X. Yang, Y. Gao, Z. Chen, K. Li, J. Qiao, T. Wang, J. Guo, C. Liu, X. Hao, H. Zhu and J. Min, *Adv. Mater.*, 2022, **34**, 2110147.

8 L. Zhan, S. Li, Y. Li, R. Sun, J. Min, Y. Chen, J. Fang, C. Q. Ma, G. Zhou, H. Zhu, L. Zuo, H. Qiu, S. Yin and H. Chen, *Adv. Energy Mater.*, 2022, **12**, 2201076.

9 T. Chen, S. Li, Y. Li, Z. Chen, H. Wu, Y. Lin, Y. Gao, M. Wang, G. Ding, J. Min, Z. Ma, H. Zhu, L. Zuo and H. Chen, *Adv. Mater.*, 2023, DOI: 10.1002/adma.202300400, e2300400.

10 Y. Guo, Z. Chen, J. Ge, J. Zhang, L. Xie, R. Peng, W. Ma and Z. Ge, *Sci. China: Chem.*, 2023, **66**, 500-507.

11 Y. Shi, L. Zhu, Y. Yan, M. Xie, G. Liang, J. Qiao, J. Zhang, X. Hao, K. Lu and Z. Wei, *Adv. Energy Mater.*, 2023, **13**, 2300458.

12 Y. Cai, Y. Li, R. Wang, H. Wu, Z. Chen, J. Zhang, Z. Ma, X. Hao, Y. Zhao, C. Zhang, F. Huang and Y. Sun, *Adv. Mater.*, 2021, **33**, 2101733.

13   X. Duan, W. Song, J. Qiao, X. Li, Y. Cai, H. Wu, J. Zhang, X. Hao, Z. Tang, Z. Ge, F. Huang and Y. Sun, *Energy Environ. Sci.*, 2022, **15**, 1563-1572.

14   H. Chen, S. Y. Jeong, J. Tian, Y. Zhang, D. R. Naphade, M. Alsufyani, W. Zhang, S. Griggs, H. Hu, S. Barlow, H. Y. Woo, S. R. Marder, T. D. Anthopoulos, I. McCulloch and Y. Lin, *Energy Environ. Sci.*, 2023, **16**, 1062-1070.

15   C. Han, J. Wang, S. Zhang, L. Chen, F. Bi, J. Wang, C. Yang, P. Wang, Y. Li and X. Bao, *Adv. Mater.*, 2023, **35**, 2208986.

16   Y. Li, Y. Guo, Z. Chen, L. Zhan, C. He, Z. Bi, N. Yao, S. Li, G. Zhou, Y. Yi, Y. Yang, H. Zhu, W. Ma, F. Gao, F. Zhang, L. Zuo and H. Chen, *Energy Environ. Sci.*, 2022, **15**, 855-865.

17   T. Ki, C. Lee, J. Kim, I. W. Hwang, C. M. Oh, K. Park, S. Lee, J. H. Kim, C. Balamurugan, J. Kong, H. S. Jeong, S. Kwon and K. Lee, *Adv. Funct. Mater.*, 2022, **32**, 2204493.

18   Y. Zeng, D. Li, H. Wu, Z. Chen, S. Leng, T. Hao, S. Xiong, Q. Xue, Z. Ma, H. Zhu and Q. Bao, *Adv. Funct. Mater.*, 2021, **32**, 2110743.

19   J. Chen, J. Cao, L. Liu, L. Xie, H. Zhou, J. Zhang, K. Zhang, M. Xiao and F. Huang, *Adv. Funct. Mater.*, 2022, **32**, 2200629.

20   X. Yuan, R. Sun, Y. Wu, T. Wang, Y. Wang, W. Wang, Y. Yu, J. Guo, Q. Wu and J. Min, *Adv. Funct. Mater.*, 2022, **32**, 2200107.

21   F. Qi, Y. Li, R. Zhang, F. R. Lin, K. Liu, Q. Fan and A. K. Jen, *Angew. Chem. Int. Ed.*, 2023, **62**, 202303066.

22   Y. Li, Y. Cai, Y. Xie, J. Song, H. Wu, Z. Tang, J. Zhang, F. Huang and Y. Sun, *Energy Environ. Sci.*, 2021, **14**, 5009-5016.

23   R. Sun, T. Wang, Y. Wu, M. Zhang, Y. Ma, Z. Xiao, G. Lu, L. Ding, Q. Zheng, C. J. Brabec, Y. Li and J. Min, *Adv. Funct. Mater.*, 2021, **31**, 2106846.